Nanomedicine: Nanotechnology, Biology, and Medicine
29 (2020) 102258

nanomedicine
Nanotechnology, Biology, and Medicine

nanomedjournal.com

Selenium nanoparticles trigger alterations in ovarian cancer cell biomechanics

Benoit Toubhans[a,b,*], Salvatore Andrea Gazze[a], Caroline Bissardon[c], Sylvain Bohic[c,d], Alexandra T. Gourlan[b], Deyarina Gonzalez[a], Laurent Charlet[b], R. Steven Conlan[a], Lewis W. Francis[a]

[a]*Centre for NanoHealth, Swansea University Medical School, Swansea, UK*
[b]*ISTerre Université Grenoble Alpes, Grenoble, France*
[c]*Inserm, UA7, Synchrotron Radiation for Biomedicine (STROBE), Université Grenoble Alpes, Grenoble, France*
[d]*ID16A Beamline, ESRF, The European Synchrotron, Grenoble, France*

Revised 22 May 2020

Abstract

High dose selenium acts as a cytotoxic agent, with potential applications in cancer treatment. However, clinical trials have failed to show any chemotherapeutic value of selenium at safe and tolerated doses (<90 μg/day). To enable the successful exploitation of selenium for cancer treatment, we evaluated inorganic selenium nanoparticles (SeNP), and found them effective in inhibiting ovarian cancer cell growth. In both SKOV-3 and OVCAR-3 ovarian cancer cell types SeNP treatment resulted in significant cytotoxicity. The two cell types displayed contrasting nanomechanical responses to SeNPs, with decreased surface roughness and membrane stiffness, characteristics of OVCAR-3 cell death. In SKOV-3, cell membrane surface roughness and stiffness increased, both properties associated with decreased metastatic potential. The beneficial effects of SeNPs on ovarian cancer cell death appear cell type dependent, and due to their low *in vivo* toxicity offer an exciting opportunity for future cancer treatment.

Key words: Selenium; Nanoparticles; Nanomechanics; Ovarian Cancer; Metastasis

Selenium (Se) is an essential trace element, obtained primarily through the diet as selenium containing amino acids,[1] however it has a narrow safe range of exposure and becomes toxic at levels above the recommended dietary intake (30-90 μg/day). Selenoproteins are implicit in human health due to their antioxidant activity and are associated, for example, with anti-inflammatory, and antiviral properties.[2] Selenocysteine (SeCys) is present in Se containing proteins, predominantly glutathione peroxidase (GPX) in the liver, and is involved in reactive oxygen species (ROS) scavenging through its redox function.[3] GPX reduces lipid hydroperoxides in alcohols and reduces free hydrogen peroxide to water.

Observational studies revealed that Se can inhibit cancer cell growth. This effect occurs through increasing ROS-mediated necrosis in prostate cancer,[4] autophagy in colorectal cancer,[5] and apoptosis in skin, breast, and liver cancer.[6] However, a meta-analysis of randomized controlled trials, >25,000 patients, failed to show any significant effect of Se dietary supplementation in reducing the incidence of colorectal, skin, lung, bladder or prostate cancer.[7] High supplementation levels induced toxicity limiting the utility of Se containing compounds as potential chemotherapeutic agents.[8] To overcome the toxicity associated with soluble Se, Se-nanoparticles (SeNPs) have been synthesized and evaluated for their anticancer properties. Both free-SeNPs[9] and encapsulated-SeNPs[10] are effective in reducing cancer cell proliferation *in vitro*. Furthermore, SeNPs appear to be effective and well tolerated *in vivo* [11], enabling Se to be used effectively at doses that would be toxic if administered as soluble Se.

Ovarian cancer is the seventh most common cancer in women with five-year survival rates of less than 45%,[8] and only 20% of cases are detected at early stages of the disease.[12] The ovarian micro-environment cancer is highly inflammatory, and the use of

The authors declare no conflict of interest.

*Corresponding author at: Centre for NanoHealth, Swansea University Medical School.
E-mail address: 970914@swansea.ac.uk. (B. Toubhans).

https://doi.org/10.1016/j.nano.2020.102258

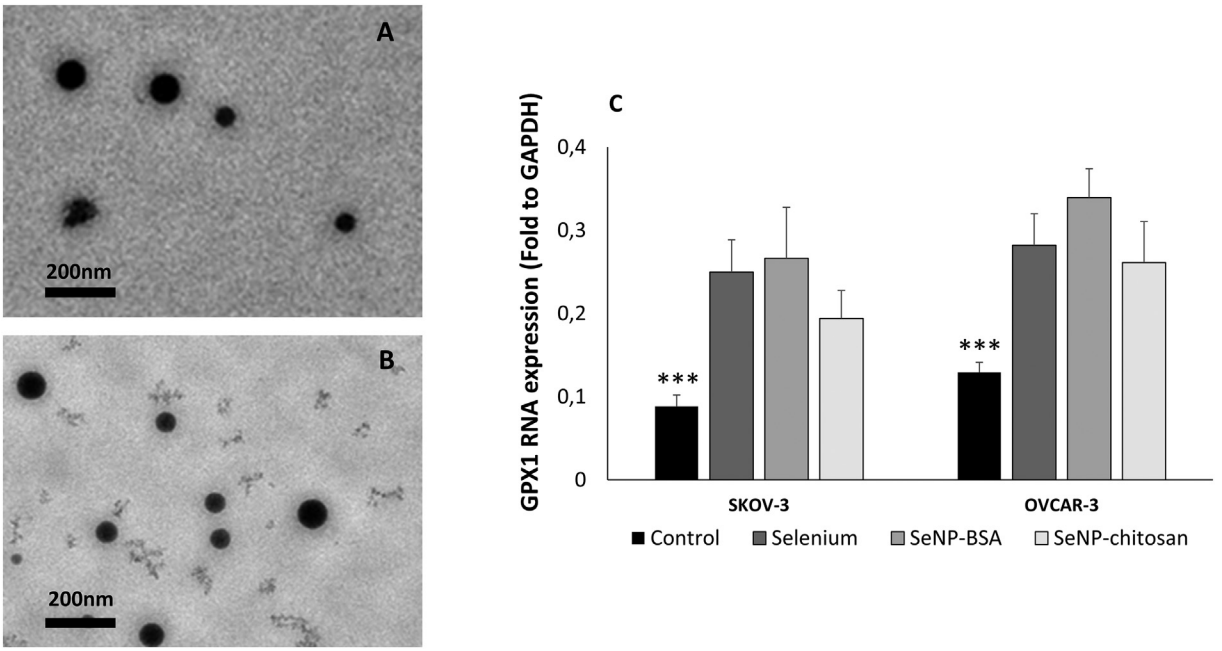

Figure 1. **SeNP characterization and internalization**. Representative TEM images of the SeNP-BSA (A) and SeNP-chitosan (B). Images have been taken with x23000 magnification. Treatment for 48 h with sublethal doses of selenite, SeNP-BSA and SeNP-chitosan resulted in significant alteration (C) in SKOV-3 (left) or OVCAR-3 (right) cells expression of GPX1. In untreated SKOV-3 relative GPX1 expression levels were respectively 0.08 +/– 0.01 for control, 0.25 +/– 0.03 for selenite, 0.26 +/– 0.06 SeNP-BSA, 0.19 +/– 0.03 for SeNP-Chitosan. Same pattern have been observed in OVCAR with 0.13 +/– 0.01 for control, 0.28 +/– 0.03 for Selenite, 0.34 +/– 0.03 SeNP-BSA, 0.26 +/– 0.05 SeNP-Chitosan. All measurement representative of a minimum 3 biological repeats.

antioxidant supplements has been correlated with a decreased risk of cancer development[13] , possible due to the form of selenite used in supplements forming endogenous SeNPs that inhibit glycolysis, causing mitochondrial dysfunction, autophagy and cytoskeletal depolymerisation.[14]

Tumor metastasis in advanced ovarian disease is the leading cause of death and is an inherently mechanical process where these properties are known to be altered.[16,17] The acquisition of invasiveness by tumor initiating cells is accompanied by the loss of the epithelial features and the gain of a mesenchymal phenotype, termed epithelial to mesenchymal transition (EMT).[15] Chemotherapeutic drugs have been shown to modify such cellular biomechanical features, through architectural changes to the cell cytoskeleton.[18] Similarly cellular cytoskeletal components such as actin microfilaments, intermediate filaments, and microtubule polymer networks play determinant roles in cellular mechanical properties, locomotion, while regulating cellular integrity during differentiation.[18] Modifications to those networks influence cytoadherence, migration, invasion and tumor metastasis.[19,20]

Here, we assessed the anticancer activity of protein (BSA) and carbohydrate (chitosan) surface coated SeNPs in two distinct high grade serous ovarian cancer cell lines, OVCAR-3 and SKOV-3. Both SeNPs were significantly more cytotoxic than soluble Se in OVCAR-3 cells at high doses (>40μg/mL), but similar to soluble Se with SKOV-3 cells, which were more sensitive to Se treatment than OVCAR-3 cells, highlighting the differences between cell types. Further analysis revealed SKOV-3 cells exhibited stable EMT markers and decreased motility, and interestingly, an increase cell surface roughness and cellular stiffness. In contrast OVCAR-3 cells displayed a decrease in cellular stiffness indicative of altered cytoskeletal dynamics that, alongside decreased vimentin expression levels and autophagy, can be interpreted as sensitization toward apoptosis.[5,6,21] It appears that reduction in cell viability following SeNP exposure occurs through different mechanisms that result in contrasting perturbations in cellular mechanics in serous ovarian cancer subtypes. SeNPs may therefore offer the potential for pan-cancer treatments, not least in ovarian cancer, that is a complex and multifaceted disease with a very poor prognostic outcome.

Methods

Cell culture

The OVCAR-3 (ATCC, Rockville, MD, USA) ovarian cancer cells were cultured in RPMI-1640 (Sigma-Aldrich, Gillingham, UK) supplemented with 20% bovine serum albumin (BSA, Sigma-Aldrich, UK), 5 μg/mL insulin (Sigma-Aldrich, Gillingham, UK), and 1% penicillin-streptomycin (v/v) solution (Sigma-Aldrich, UK). The SKOV-3 (ATCC, Rockville, MD, US) ovarian cancer cells were cultured in McCoy's 5A (Sigma-Aldrich, Gillingham, UK) supplemented with 10% bovine serum albumin (BSA, Sigma-Aldrich, UK), and 1% penicillin-streptomycin (v/v) (Sigma-Aldrich, Gillingham, UK). Cells were maintained at 37°C and 5% CO_2 and routinely passaged using 0.25% trypsin - 0.1% EDTA (v/v).

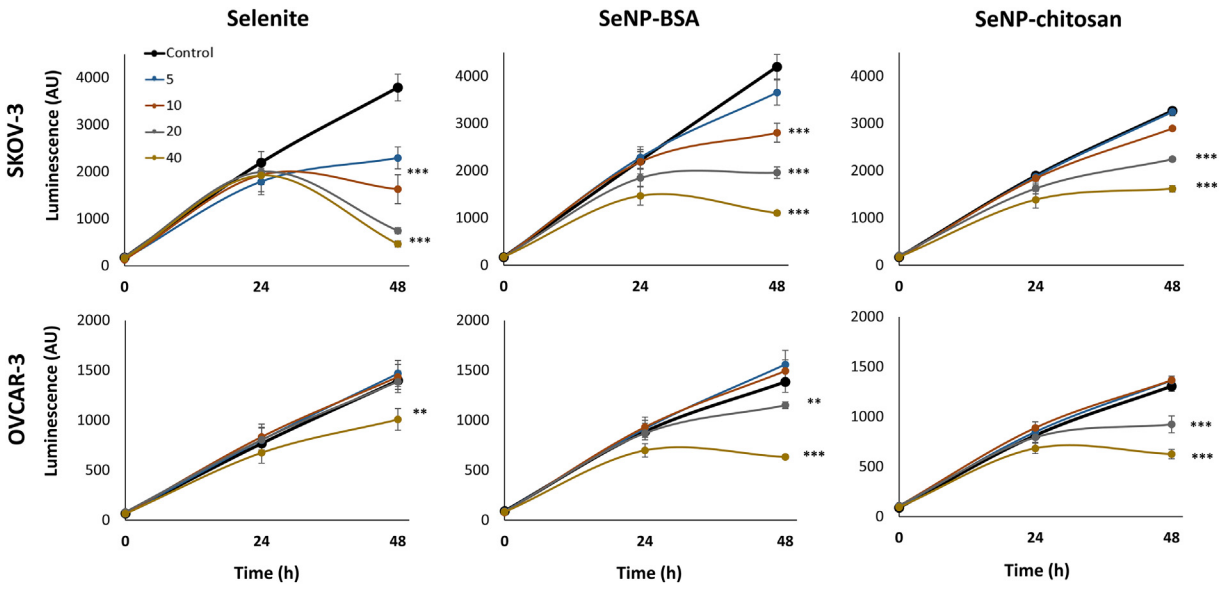

Figure 2. **SeNP cytotoxicity**. Ovarian cancer cells SKOV-3 (top) and OVCAR-3 (bottom) were grown in the presence of Selenite, BSA coated selenium nanoparticles or chitosan coated selenium nanoparticles over 48 h and monitored for cellular cytotoxicity. Both cell lines were treated for 48 h with an increasing range of concentration from 0 to 80 μg/mL. Cytotoxicity was evaluated by RTGlo and mean (+/−SD) luminescence values shown) from four independent experiments. SKOV-3 and OVCAR-3 viability are presented in comparison with control in supplementary figure 1.

SeNP characterization

SeNPs were purchased from NANOCS (New York, USA) with two different coatings, BSA and chitosan. Manufacturer specifications stated 25 – 50 nm of diameter for both nanoparticles. Size shape and charge analysis was conducted by Dynamic Light Scattering and Zeta Potential measurement using a ZetaSizer Nano (Malvern Instruments, Malvern, UK) with a 173° scattering angle using SeNPs at 1μg/mL in water (reflexive index of 1.33) at 25°C.

Cell growth and Se treatment

Both SKOV-3 and OVCAR-3 cells were cultured in growth medium until 80% confluency, trypsinized per regular passage and seeded to sterile petri dishes (Corning, UK) at 37° C and 5% CO_2. After 48 h incubation culture medium was removed and 2 mL of fresh medium containing the expected concentration of aqueous Se (selenite Se^{4+}) or SeNPs added for a further 48 h prior to analysis, with a minimum of three biological repeats.

Cell viability assay

Ovarian cancer cell viability in the presence and absence of Se treatments was determined using the Real-Time Glo assay (RTGlo, PROMEGA, Southampton, UK). 1×10^3 ovarian cancer cells/well were plated within 96-well white plates (Corning, UK). After 24 h of growth, culture media was aspirated and 100 μL of fresh medium containing aqueous Se (selenite Se^{4+}) or SeNPs (BSA or chitosan) were added. An increasing dose range (0.06 μg/mL to 40 μg/mL) was applied by dilution in appropriate medium for 48 h. The RTGlo with RPMI-1640 medium was added 1:1 with treatment medium. A BMG Labtech Fluostar Omega was used to measure luminescence every 24 h and presented as absolute values. IC20/IC50 doses were determined as the concentration of treatment that reduced by 20%/50% the luminescence signal compared to untreated control. The IC20/IC50 values shown (average ± standard deviation) are from a minimum of four independent experiments performed with 6 technical repeats.

Migration assay

2×10^5 SKOV-3 cells/per well were seeded in 12 well plates and cultured in complete culture medium until the cells reached confluence. A scratch was then introduced to the monolayers, using a sterile (20 μL pipette) tip. The media was then aspirated and a fresh, fetal bovine serum (FBS, Gibco, UK) free medium containing IC20 selenium treatment was added to each well and cultured for 48 h. The scratch was imaged at 0, 24, 48 h using a Primo Vert inverted light microscope (Zeiss, Cambridge, UK). Average scratch width measurements were measured at three random areas, in three wells for each condition, as previously reported.[22] The migration rate was calculated according to the following equation: cell motilities (%) = [1 − (distance of scratched area at 24 h/distance of scratched area at 0 h)] ×100%.

Protein blotting

Total cellular protein was extracted using TRIzol™ reagent (Sigma, Gillingham, UK) and quantified using the DC™ Protein Assay (BioRad, Deeside, UK). Protein from each sample was mixed with Laemmli sample buffer containing β-mercaptoethanol (5%) and boiled at 95°C for 5 min. Equal

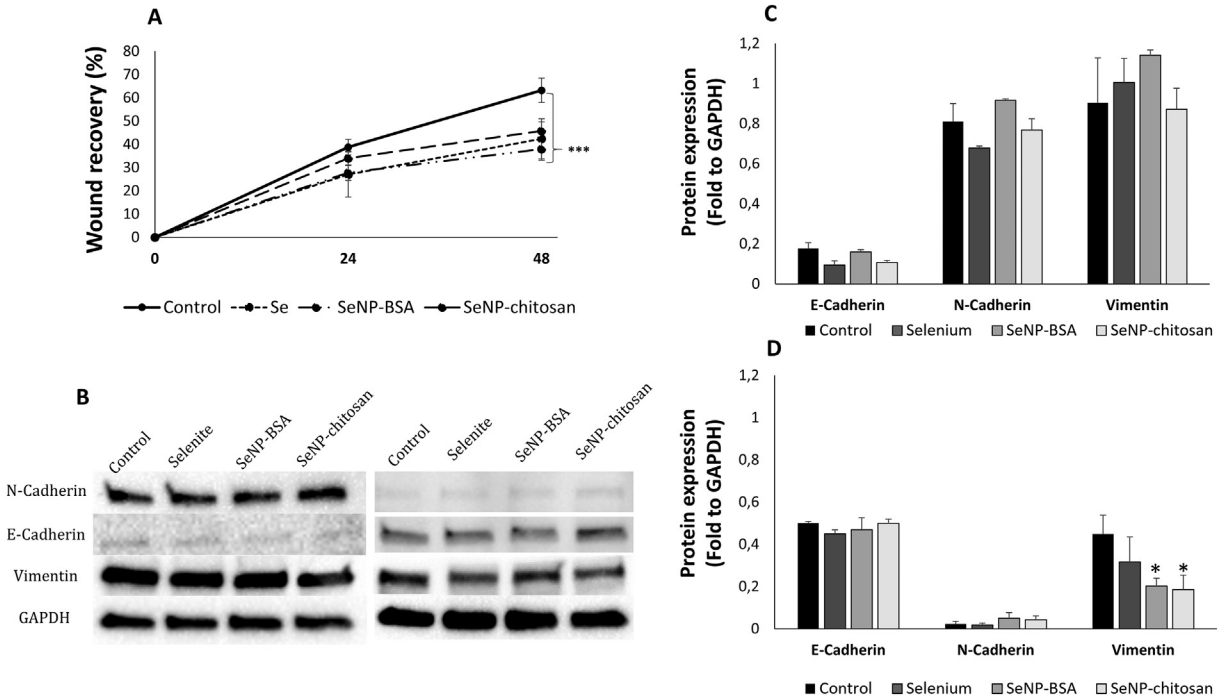

Figure 3. **Effect of SeNPs on EMT phenotype.** Scratch/wound healing assay (A) results showed that selenite, SeNP-chitosan and SeNP-BSA treatments at IC20 significantly decreased migration of SKOV-3 cells during 48 h. SeNP-BSA treatment decreases the recovery rate by 25% (+/–4.8%), SeNP-chitosan treatment by 16.5% (+/–3.8%) and selenite treatment by 18.6 (+/–8.2%) in comparison with control ($P < 0.05$). It was not possible to complete the migration assay with OVCAR-3 cells as they do not survive when depleted with FBS. Treatment for 48 h with IC20 selenite, SeNP-BSA and SeNP-chitosan resulted in no significant alteration in SKOV-3 or OVCAR-3 cells profiling of EMT markers (E-cadherin, N-cadherin, Vimentin) (C, D). In untreated SKOV-3 (C) relative vimentin expression levels were similar between conditions with respectively 0.9 (+/–0.2) for control, 1.01 (+/–0.1) for selenite, 1.14 (+/–0.02) for BSA SeNP, 0.87 (+/–0.11) for chitosan SeNP. Relative expression of E-cadherin was low (0.01 to 0.02). N-cadherin expression was similar between conditions with respectively 0.8 (+/–0.08) for control, 0.67 (+/–0.01) for selenite, 0.9 (+/–0.01) for BSA SeNP, 0.76 (+/–0.05) for chitosan SeNP. In untreated OVCAR-3 (D) relative vimentin expression levels were 0.45 (+/–0.08) while it was decreased in treated cells with 0.31 (+/–0.1) with selenite, 0.20(+/–0.03) for BSA SeNP and 0.18(+/–0.06) for chitosan SeNP. Relative expression of N-cadherin was very low (0.02 to 0.05). E-cadherin expressions were the same between the different conditions with 0.50 (+/–0.05) for control, 0.45 (+/–0.2) for selenite, 0.47 (+/–0.05) for SeNP-BSA and 0.5 (+/–0.002) for chitosan SeNP. Examples of western blots have been displayed in (B).

amounts of protein (30 µg) were separated by SDS-PAGE (4-20% gels) and subsequently transferred onto a PVDF membrane (Biorad, Deeside, UK). The membranes were blocked for 1 h in 5% BSA prepared in 0.1% Tris-buffered saline-Tween20® (TBS-T). Blots were then incubated with the corresponding primary antibody (E-cadherin: mouse monoclonal (Abcam ab1416, Cambridge, UK), vimentin: mouse monoclonal (Santa Cruz sc-6260, Wembley, UK), N-cadherin: rabbit polyclonal (Abcam ab18203, Cambridge, Wembley, UK) or GAPDH: mouse monoclonal (Santa Cruz sc-47724, Wembley, UK)) at a concentration of 200 µg/mL overnight at 4°C. Blots were then washed 3 times with TBS-T and incubated at room temperature for 1 h with the appropriate secondary antibody (goat anti-mouse Abcam ab150113 or goat anti-rabbit Abcam ab6721 HRP secondary, Cambridge, UK) at a concentration of 400 µg/mL. For signal detection, membranes were processed using the Clarity™ Western ECL Substrate kit (BioRad, Deeside, UK) according to the manufacturer's recommendations and visualized using a ChemiDoc XRS system (BioRad, Deeside, UK). Analysis of the intensity of the bands was done using Image Lab (BioRad, Deeside, UK) software tracing fixed size-limited rectangle around the bands of interest and reporting the Adjusted Volume (Intensity corrected by the background noise). Protein expression was normalized GAPDH and relative expression expressed as the mean fold induction ± standard deviation.

qRT-PCR

Following RNA extraction and quantification, qPCR was carried out in accordance with the manufacturers' recommendations, using the RETROscript® kit two-step method (Invitrogen Ltd., UK). Following cDNA synthesis from 100 ng of RNA, each sample was analyzed by qPCR in triplicate using iQ SYBR Green supermix (BioRad, Deeside, UK) and gene specific primers (Sigma-Aldrich, Gillingham, UK) to evaluate different gene expression GAPDH (GAPDH Forward: GTCCACTGGCGTCTTCAC, Reverse: CTTGAGGCTGTTGTCATACTTC) and GPX1 (GPX1 Forward: GTGCTCGGCTTCCCGTGCAAC, Reverse: CTCGAAGAGCATGAAGTTGGGC). Serial dilutions of cDNA were used to plot a calibration curve, and gene expression quantified

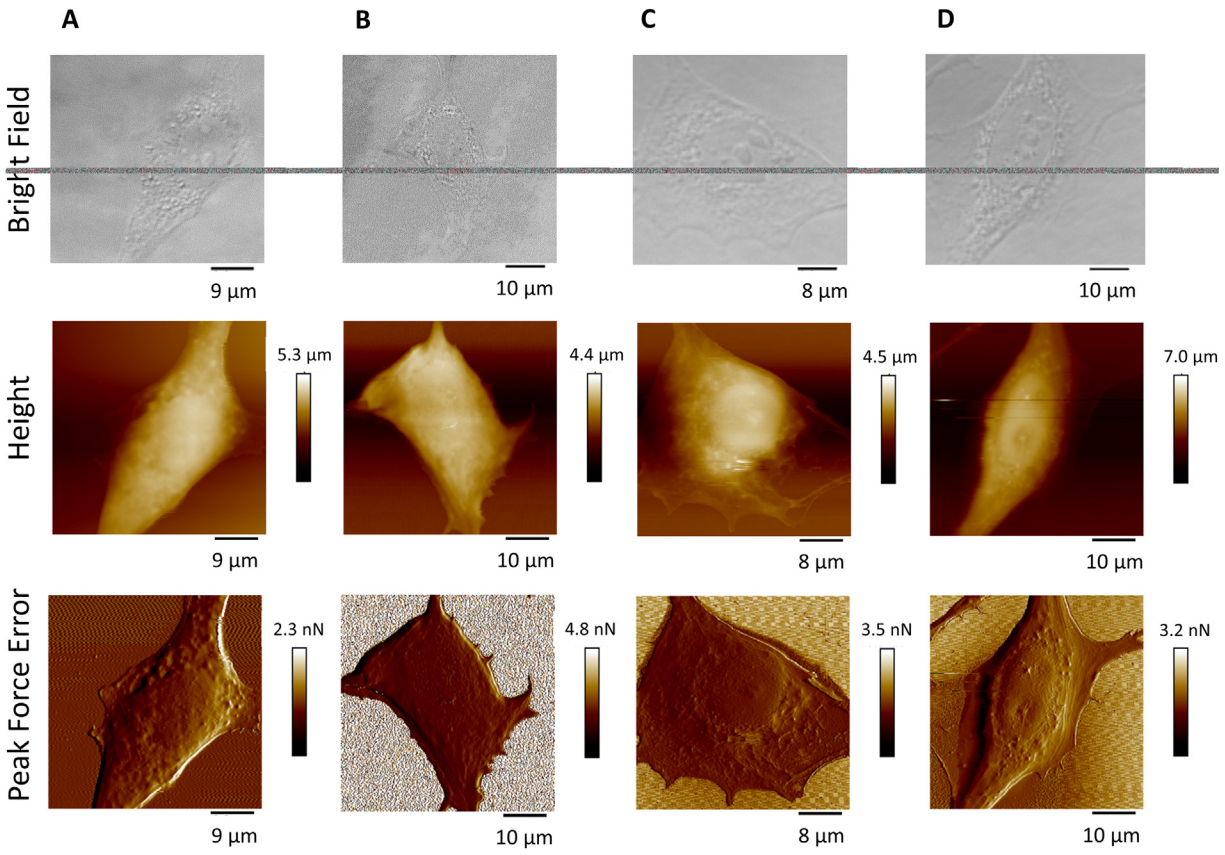

Figure 4. **Effect of SeNP on SKOV-3 morphology and topography.** SKOV-3 cells were treated with Se-NPs for 48 h and compared to selenite (IC20) and an untreated control. High resolution AFM imaging was performed and subsequent image analysis. No morphological and/or topographical cell changes were detected with stable morphological features observed in the Control (A), IC20 Selenite (B), IC20 BSA coated SeNP (C), IC20 chitosan coated SeNP (D) using bright field, AFM height and PeakForce error signal respectively. The shown image is representative of the morphology of SKOV-3, from imaging 15 cells from 3 biological repeats.

by plotting threshold cycle values. Expression levels were normalized to values obtained for the reference gene (GAPDH) and relative expression expressed as the mean fold induction ± standard deviation. Statistical differences between the treatment groups and the control were determined by analysis of variance (ANOVA) (where $P < 0.05$ was considered significant).

AFM analysis

Young modulus, indentation and adhesion

Force-indentation curves were obtained using a Nanowizard II AFM (JPK, Berlin, Germany) mounted on a ZEISS 510 confocal microscope (Zeiss, Cambridge, UK) as described in[23]. During AFM, cells were kept alive in serum free, pH indicator free culture media at 37°C in a petri dish using a standard stage heater and analyzed for a maximum of 3 h. The inverted optical microscope was used to position the tip on the cell and force volume conducted using borosilicate colloidal (Novascan, UK) cantilevers, with a nominal spring constant of 0.35 N/m with a radius of 2.5 µm. Prior to measurements, deflection sensitivity and spring constant were experimentally determined, the latter using the subroutine of the JPK software. Three individual force curves (ramp size of 6 µm) were taken on a total of 25 cells, across 3 independent biological experiments, using a maximum force indentation of 6 nN was used. JPK Data Processing program was used to process the acquired force curves. For each force curve the baseline was corrected to 0 and the approach curve in the contact regime of each force curve was fitted using the classical Hertz model according to Eq. 1. In both cases, the fitting module in the JPK software was used and only curves with a goodness of fit between 0.85 and 1 were considered for statistical analysis.

$$R_{RMS} = \sqrt{\frac{\sum Z_i^2}{N}} \tag{1}$$

In this equation, F is the force applied by the cantilever tip to the cell, E is the Young's modulus (fit parameter), υ is the Poisson's ratio (0.5), R the radius of the indenter, δ is the indentation depth and α is the half-angle of the indenter (18° for the used sharp probes).

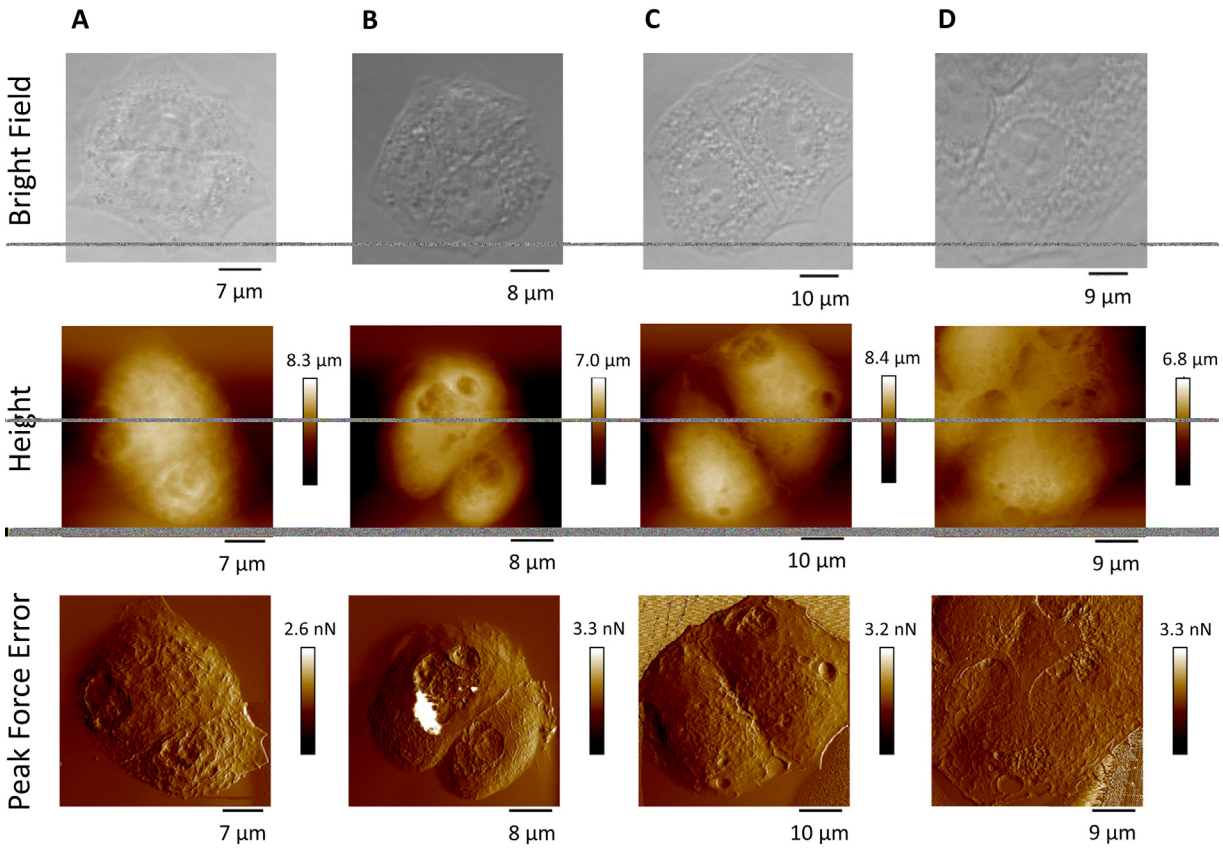

Figure 5. **Effect of SeNP on OVCAR-3 morphology and topography.** OVCAR-3 cells were treated with Se-NPs for 48 h and compared to selenite (IC20) and an untreated control. High resolution AFM imaging was performed and subsequent image analysis. No morphological and/or topographical cell changes were detected with stable morphological features observed in the Control (A), IC20 selenite (B), IC20 BSA coated SeNP (C), IC20 chitosan coated SeNP (D) using bright field, AFM height and PeakForce error signal respectively. The shown image is representative of the morphology of OVCAR-3, from imaging 15 cells from 3 biological repeats.

Topography and surface roughness

In order to resolve the membrane architecture, cells were fixed for imaging according to the protocols outlined in Francis et al. [24] Briefly cells were washed 2 times with PBS then fixed for 30 min in 4% PFA (Merck, UK) diluted in PBS at RT. PFA was subsequently removed and replaced by phosphate buffered saline (PBS), at RT. SKOV-3 and OVCAR-3 cell morphology and topography were analyzed using a BioScope Catalyst (Bruker Instruments, USA) mounted on a Nikon Eclipse Ti-S inverted optical microscope (Nikon Instruments, Netherlands). The inverted optical microscope was used to carefully position the tip on the desired cell and tapping mode imaging undertaken using MLCT-E silicon nitride cantilevers (Bruker-Nano, UK). Offline processing for AFM height data consisted of first-order flattening and plane fitting. The membrane roughness was measured using the subroutine in the Nanoscope Analysis software v1.50, on areas of 25 μm^2 each on five cells for control and treated, from a minimum of 3 biological repeats. Membrane roughness was calculated using Eq. 2,

$$R_{RMS} = \sqrt{\frac{\sum Z_i^2}{N}} \quad (2)$$

where N is the number of height points in the analyzed area and Zi is the vertical distance of data point i from the mean image data plane. Sixteen roughness measurements were calculated per image, with 1 μm^2 areas of measurement.

Statistical analysis

All data presented are calculated from a minimum of three biological repeats, with technical repeats included per sample, as denoted. Data normality was analyzed using the Kolmogorov Smirnov test, with normally distributed data analyzed with the one-way and two-way analysis of variance (ANOVA) or the Mann–Whitney pairwise test for non-parametric data. In all cases in which ANOVA was significant, multiple comparison methods were used. Differences were considered significant for $P \leq 0.05$ ($^*P \leq 0.05$, $^{**}P \leq 0.01$, $^{***}P \leq 0.001$). All data were analyzed in MiniTab 14.

Results

Physicochemical and biological characterization of SeNPs

Based on previous observations showing Se has anti-proliferative effects on ovarian cancer cells,[14,25,26] and the good tolerability of

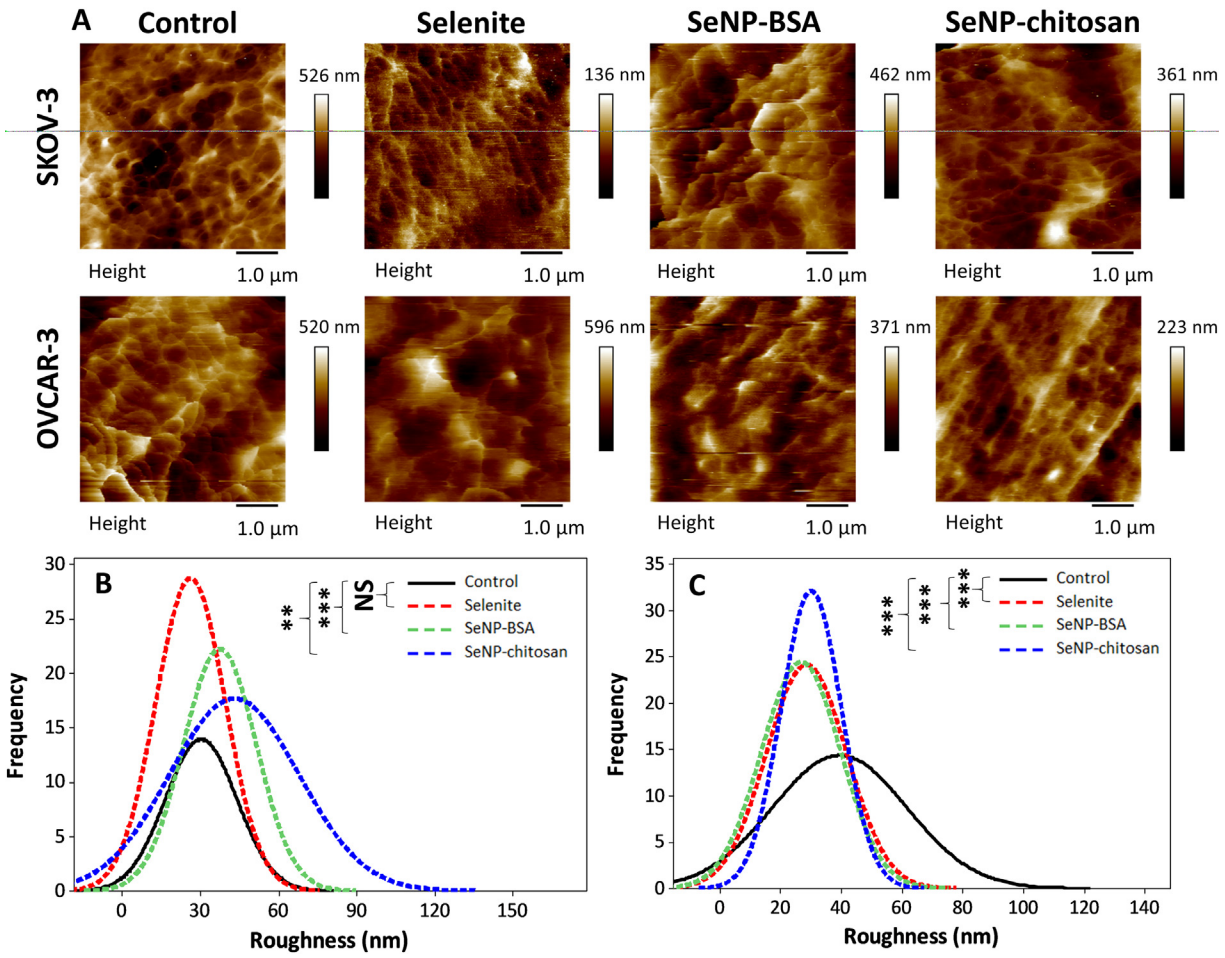

Figure 6. **Effect of SeNP on SKOV-3 and OVCAR-3 surface roughness.** Cell roughness (SKOV-3 (B) and OVCAR-3 (C)) was calculated on height cells with 25µm^2 areas measurement and 1µm^2 analysis squares in all groups. Images of example areas are displayed in A. SKOV-3 control cell surface roughness (R_{RMS}= 33.08 +/− 1.56 nm) was similar with selenite treated cells (R_{RMS}=26.41 +/− 1.15 nm) and significantly lower than observed in SeNP treated cells (R_{RMS}=37.31 +/− 1.58 nm for BSA and R_{RMS}=42.89 +/− 2.37 nm for Chitosan). OVCAR-3 control cell surface roughness (R_{RMS} =39.39 +/− 2.48 nm) was significantly higher than that observed in treated cells (R_{RMS}=28.41 +/− 1.82 nm in selenite treated cells, R_{RMS}=27.92 +/− 1.75 nm in BSA coated SeNP treated cells and R_{RMS}= 30.05 +/− 1.11 nm in chitosan coated SeNP).

SeNPs *in vivo* in other disease models[27,28] we evaluated cytotoxicity of BSA and chitosan coated SeNP on SKOV-3 and OVCAR-3 cells. Characterization of SeNPs (see supplementary figure 2) aggregation and charge demonstrated SeNP-BSA had a negative charge (-51.2 ± 15.8 mV) and an average size of 108 ± 30 nm and PDI of 0.123 ± 0.002 which was considered monodisperse, and the 30-100 nm size range confirmed by transmission electron microscopy (TEM) (Figure 1, *A* and *B*). SeNP-chitosan had a positive charge of 16.4 ± 4.4 mV, an average size of 320 ± 221 nm and PDI of 0.220 ± 0.012 and was considered as polydisperse.[29] SeNP-chitosan size values with the ZetaSizer measurement were higher than the supplier's specification of 50nm average size however TEM images confirmed those specifications (Figure 1, *A* and *B*)

To demonstrate that SKOV3 and OVCAR3 cells were responding to Se treatments, and therefore confirming that Se had been effectively taken up by cells, GPX1 mRNA levels were measured.[30] GPX mRNA levels increased 2-2.5-fold following Se treatment in both cell types (Figure 1, *C*).

Ovarian cancer cell line dependent SeNP cytotoxicity

SKOV-3 and OVCAR-3 cell monolayers were treated with increasing concentrations of SeNP-BSA, SeNP-chitosan or sodium selenite (0 – 80 µg/mL) over 48 h and cell viability measured. For SKOV-3 (Figure 2) cells selenite treatment had a greater cytotoxic than SeNP-BSA and SeNP-chitosan. The IC20 for selenite was 3 µg/mL at 48 h (Figure 2), whereas the IC20 for SeNP-BSA and SeNP-chitosan were 6 µg/mL and 13 µg/mL respectively ($P < 0.05$). Above 5µg/mL of selenite, SKOV-3 cell viability was significantly reduced compared to untreated control after 48 h ($P < 0.05$). Whereas for SeNP-BSA and SeNP-chitosan the concentration required to cause a significant reduction in cell viability was 10 µg/mL and 20 µg/mL respectively ($P < 0.05$).

In contrast, OVCAR-3 cells were more sensitive to both types of nanoparticles than selenite (Figure 2), the IC20 at 48 h was not significantly different between SeNP-BSA and SeNP-chitosan treatment at 20 μg/mL and 18 μg/mL respectively ($P > 0.05$), whereas the IC20 for selenite was 40 μg/mL (Figure 2, $P < 0.05$).

IC50 values confirmed SKOV-3 cells were more sensitive than OVCAR-3 to both selenite and SeNP-BSA treatments (8 vs 56 μg/mL and 19 vs 42 μg/mL respectively, $P< 0.05$), whereas the IC50 for SeNP-chitosan the same (40 μg/mL) for both SKOV-3 and OVCAR-3 (Figure 2, *B* and *C*). It appears that selenite has a greater cytotoxic effect on SKOV-3 cells than SeNPs, whereas the opposite was observed for OVCAR-3 cells, which are more sensitive to SeNPs than selenite. The concentrations of SeNPs required to decrease cell viability are all significantly higher in OVCAR-3 than SKOV-3 suggesting that the two cell types are responding differently to Se treatment despite the GPX stimulation being similar.

Epithelial–mesenchymal transition (EMT) is a cellular mechanism linked to differentiation during cancer progression,[31] and includes alterations in E- and N-cadherin and vimentin expression, and increased cell migration.[32] Efforts to reverse these transitions are an important consideration in treating aggressive cancers. The effect of Se on cell motility was assessed using a scratch assay, treating cells with IC20 levels of selenite and SeNPs for 48 h. Motility rates were decreased by 25% following SeNP-BSA treatment, 17% after SeNP-chitosan treatment and 19% with selenite ($P < 0.05$, Figure 3, *A*), suggesting that whilst selenite was move cytotoxic the three treatments has a similar extent in reducing cell motility. Scratch assays were not possible with OVCAR-3 cells as these cells do not survive when depleted with FBS. In SKOV-3 cells assessment of EMT markers revealed that selenite and SeNPs had no effect with E-cadherin expression remaining at very low levels, and N-cadherin and vimentin remaining highly expressed consistent with an unaltered mesenchymal phenotype. (Figure 3, *B* and *C*. In OVCAR-3 cells the E-cadherin:N-cadherin was the opposite to that observed in SKOV-3 cells suggestive of a more epithelial phenotype (Figure 3, *B* and *D*), however neither marker responded to selenium treatments. In contrast, vimentin levels significantly ($P < 0.05$) decreased following treatment with SeNPs, an effect that has previously been correlated with a decrease in cancer cell mechanical integrity.[18]

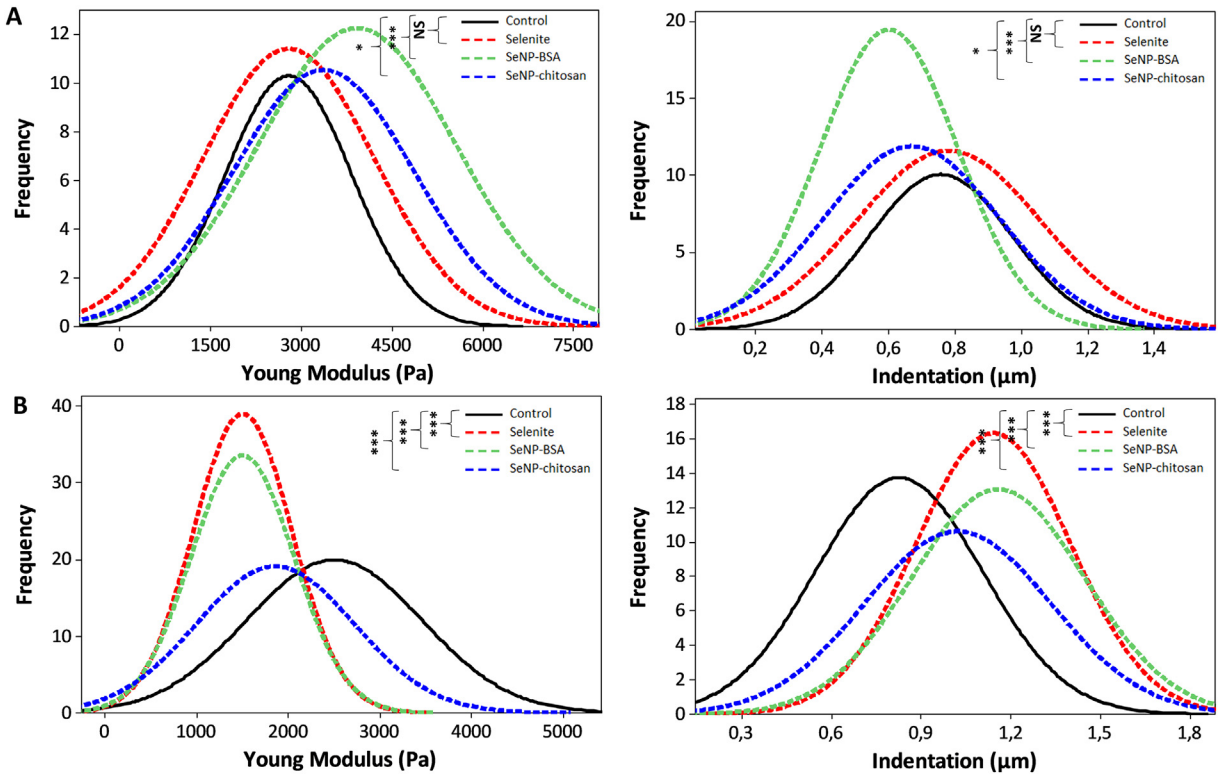

Figure 7. **Effect of SeNP on SKOV-3 and OVCAR -3 cell stiffness and nano-indentation.** AFM probe with a colloidal tip was used as a nano-indentor to monitor changes in cell elasticity following 48 h of treatment. Using Hertz mechanics, elasticity was calculated from the observed changes in the contact regime of the force curve. The 0 point in the x-axis indicates when the cantilever tip makes contact with the cell surface. Total cell elasticity values are drawn in frequency curve for control and treated cells at 48 h. Highly significant alterations in median values were detected between control and treated cells. Indentation data reported that were applying the same force results in treated OVCAR-3 (B) cells deforming more than control cells. SKOV-3 (A) cells seem to deform less after treatment. Statistical significance was determined using the Mann-Whitney test with the following used symbols NS=$P > 0.05$, *$P < 0.05$ **$P < 0.01$, ***$P < 0.001$.

Effect of SeNP treatment on surface roughness and biomechanics

Previously ovarian cancer cell biomechanics have been shown to differ depending on the invasive potential of cells,[16] and perturbations in gene expression patterns linked to enhanced cellular movement, migration, and invasion.[17] Given the decreases in motility rates described above we reasoned that this may be linked to altered biomechanical properties following SeNP exposure. Using high-resolution tapping mode AFM we initially resolved gross cellular morphology and nanoscale surface topography.

SKOV-3 had an elongated, mesenchymal like, morphology and a smooth membrane ultrastructure that remained unaltered following treatment (Figure 4, all panels). No significant change in cell height was observed between untreated cells (2.4 ± 0.3 μm) and those treated with selenite (2.8 ± 0.6 μm), SeNP-BSA (2.7 ± 0.3 μm) or SeNP-chitosan (2.3 ± 0.8 μm).

OVCAR-3 cells had a spherical, epithelial like morphology that remained unaltered following SeNP treatment (Figure 5, all panels) consistent with the observed N-cadherin and E-cadherin expression ratios. No significant changes in the height of OVCAR-3 were observed between untreated (5.2 ± 0.6 μm) and selenite (4.8 ± 0.4 μm), SeNP-BSA (5.1 ± 0.5 μm) or SeNP-chitosan (4.0 ± 0.5 μm) treated cells ($P > 0.05$; Figure 5). An increase in intra-cellular vesicles was apparent in cells with all Se treatments in bright filed images.

Membrane topography is sensitive to changes of both physical or chemical factors, and NP exposure has been shown to modulate cell membranes.[33] To investigate any SeNP effects on membrane roughness, $1\mu m^2$ areas of the cell surface selected at random from a 25 μm^2 image area and analyzed for roughness. Surface roughness increased in SKOV-3 cell treated with SeNP-BSA (37.31 ± 1.58 nm) and SeNP-chitosan (42.89 ± 2.37 nm), compared to untreated cells (33.08 ± 1.56 nm), whereas no change was detected following selenite treatment (26.41 ± 1.15 nm) ($P > 0.05$, Figure 6). For OVCAR-3 cells the surface roughness of SeNP treated was significantly decreased from 39.39 ± 2.48 nm in untreated controls to 28.41 ± 1.82 nm with selenite, 27.92 ± 1.75 nm with SeNP-BSA, and 30.05 ± 1.11 nm with SeNP-chitosan treatment ($P < 0.05$). There was no significant difference in OVCAR-3 surface roughness was observed between selenite and SeNP treatments ($P > 0.05$, Figure 6).

The mechanical properties of cells change during cancer progression, with metastatic cells becoming more elastic[17] after initial transformation to enable basement membrane penetration.[34–36] To investigate whether Se treatment resulted in any changes in cell elasticity, both SKOV-3 and OVCAR-3 cells were characterized using AFM based nanoindentation, with a colloidal probe (Figure 7).

A significant increase in cell stiffness was observed for SKOV-3 cells following treatment with either SeNP-BSA (3.9 ± 0.2 kPa) or SeNP-chitosan (3.4 ± 0.1 kPa) compared to control (2.8 ± 0.1 kPa; $P < 0.05$), whereas no alterations were detectable following selenite treatment (2.8 ± 0.2 kPa; $P > 0.05$). Indentation analysis revealed a significant decrease for SeNP treated SKOV-3 cells (Figure 7, *A*) with 600 ± 20 nm ($P < 0.001$) for SeNP-BSA and 668 ± 30 nm ($P < 0.05$) for SeNP-chitosan in comparison with control (756 ± 30 nm) and selenite treated cells (780 ± 31 nm). In OVCAR-3 cells the Young's modulus was decreased following SeNP-BSA (1.5 ± 0.1kPa), SeNP-chitosan (1.9 ± 0.1kPa) or selenite (1.5 ± 0.1kPa) treatment compared to the untreated control (2.5 ± 0.1kPa; $P < 0.001$), which together with significantly increase in cell indentation (Figure 7, *B*) following each treatment (selenite 1,141 ± 25 nm, SeNP-BSA 1,157 ± 29 nm, SeNP-chitosan 1,021 ± 34 nm) demonstrated that cell membranes had become more deformable in comparison with control (825 ± 28 nm, $P < 0.001$). Example typical force curves have been collected and are shown in Supplementary Figure 3.

Cellular adhesion to the AFM probe was also analyzed, with no significant alterations in SKOV-3 or OVCAR-3 cells respectively, as shown in Supplementary Figure 4.

Discussion

Despite the anticancer properties associated with selenium, its use as a cancer therapy has not yet been realized due to systemic toxicity when administered in an aqueous form. Here we demonstrated that, like selenite, SeNPs are effective at inducing a cytotoxic effect on two different serous ovarian cancer derived cell lines and observed distinct responses for each cell type. Both selenite and SeNPs were cytotoxic to SKOV-3 cells, with selenite having a 2.5- and 5- fold lower IC50 than SeNP-BSA and SeNP-chitosan respectively. However, given that aqueous selenium is significantly more toxic when administered systemically in murine models,[5,27,28] the use of SeNP-BSA is likely to provide an opportunity to deliver cytotoxic doses of Se *in vivo*. In addition, tumor specific delivery could occur through the enhanced permeability and retention effect,[37] further reducing toxicity. For OVCAR-3 cells SeNP-BSA and SeNP-chitosan had an approximately 2-fold greater cytotoxic effect than selenite. Given the above considerations, and that the IC50 for SeNPs in OVCAR-3 cells was almost five times greater than for SKOV-3 cells, both types of SeNP are likely to be the only safe and tolerable route for Se administration to target cancer cell growth *in vivo*.

Changes in cell mobility in SKOV-3 led us to investigate cell membrane dynamics in response to selenium treatment as we and others have previously observed differences in ovarian cancer cell biomechanics which were dependent on the invasive potential of cells,[16] and associated with genes involved in enhanced cellular movement, migration, and invasion.[17] Detailed AFM analysis revealed that SKOV-3 cells become less elastic following SeNPs treatment but remained unchanged when treated with selenite. This suggests that SeNPs are triggering a mechanism that results in a lower metastatic potential, and in agreement with the reduced migratory capacity of these cells following treatment.[20,22] In contrast, AFM analysis revealed that OVCAR-3 cells became more elastic following treatment with the higher IC20 concentrations of SeNP and selenite required to induce a cytotoxic effect with these cells. These results highlight specific differences in membrane architecture between SKOV-3 and OVCAR-3 and indicate that SeNP treatment can cause differential cell type specific cytoskeletal effects.

Further contrasting effects were seen with surface roughness, which increased following SeNP treatment in SKOV-3 cells, possibly as a result of nanoparticle internalization as previous studies have shown that BSA coated SeNPs, similar to those used in the present study, were internalized through endocytosis or clathrin mediated vesicles.[38–40] As selenite would be expected to be taken up by anion transporters[41] this difference in surface roughness was anticipated. Surprisingly, the surface roughness of OVCAR-3 cells decreased following SeNPs and selenite treatment and was accompanied by the appearance of intracellular vesicles which are likely to be autophagosomes (Figure 5, *B–D*).[42,43] This suggests that, uniquely, Se forms may induce autophagy which would act as a resistance mechanism in OVCAR-3 cells[41] and offers an explanation as to why the levels of SeNPs required to illicit a response is higher for these cells. This detailed nanomechanical assessment of two distinct ovarian cancer cell types has established that changes in the mechanical properties of ovarian cancer cells, which are likely to result from reorganization of the actin cytoskeleton induced by selenium. SeNPs are effective at preventing cell proliferation in high grade serous ovarian cancer cells, apparently through different biological pathways. High grade serous ovarian cancers continues to present obstacles to currently available treatment through the presentation of advanced and highly aggressive forms of the disease, resulting in a high rate of mortality.[8] The observations made here pave the way for further investigations into evaluating the utility of SeNPs as a pan-cancer treatment, at least in ovarian cancer, although Se is known to be effective in many other cancer types.

Acknowledgments

This project received support from the Welsh Government ERDF SMART Expertise grant RISE (2017/COL/001), the Medical Research Council UK Confidence in Concept grant (MC_PC_19053) and the Institut National de la Santé et de la Recherche Médicale, France, grant SEDMAC (PC201607).

Benoit Toubhans received a scholarship co-funded by the Université Grenoble Alpes and Swansea University.

Appendix A. Supplementary data

Supplementary data to this article can be found online at https://doi.org/10.1016/j.nano.2020.102258.

References

1. Fernandes AP, Gandin V. Selenium compounds as therapeutic agents in cancer. *Biochim Biophys Acta* 1850;**2015**:1642-60.
2. Combs F. J. Biomarkers of selenium status. *Nutrients* 2015;**7**:2209-36.
3. Khurana A, Tekula S, Saifi MA, Venkatesh P, Godugu C. Therapeutic applications of selenium nanoparticles. *Biomedicine & Pharmacotherapy* 2019;**111**:802-12.
4. Sonkusre P, Cameotra SS. Biogenic selenium nanoparticles induce ROS-mediated necroptosis in PC-3 cancer cells through TNF activation. *Journal of Nanobiotechnology* 2017;**15**:43.
5. Huang G, Liu Z, He L, Luk K-H, Cheung S-T, Wong K-H, et al. Autophagy is an important action mode for functionalized selenium nanoparticles to exhibit anti-colorectal cancer activity. *Biomater Sci* 2018;**6**:2508-17.
6. Chen T, Wong Y-S. Selenocystine induces reactive oxygen species-mediated apoptosis in human cancer cells. *Biomed Pharmacother* 2009;**63**:105-13.
7. Vinceti M, Filippini T, Del Giovane C, Dennert G, Zwahlen M, Brinkman M, et al. Selenium for preventing cancer. *Cochrane Database Syst Rev* 2018;**1**CD005195.
8. Webb PM, Jordan SJ. Epidemiology of epithelial ovarian cancer. *Best Pract Res Clin Obstet Gynaecol* 2017;**41**:3-14.
9. Geoffrion LD, Hesabizadeh T, Medina-Cruz D, Kusper M, Taylor P, Vernet-Crua A, et al. Naked selenium nanoparticles for antibacterial and anticancer treatments. *ACS Omega* 2020;**5**:2660-9.
10. Song X, Chen Y, Zhao G, Sun H, Che H, Leng X. Effect of molecular weight of chitosan and its oligosaccharides on antitumor activities of chitosan-selenium nanoparticles. *Carbohydr Polym* 2020;**231**:115689.
11. Shahverdi AR, Shahverdi F, Faghfuri E, Reza Khoshayand M, Mavandadnejad F, Yazdi MH, et al. Characterization of folic acid surface-coated selenium nanoparticles and corresponding in vitro and in vivo effects against breast cancer. *Arch Med Res* 2018;**49**:10-7.
12. Zaorsky NG, Churilla TM, Egleston BL, Fisher SG, Ridge JA, Horwitz EM, et al. Causes of death among cancer patients. *Ann Oncol* 2017;**28**:400-7.
13. Bertone ER, Hankinson SE, Newcomb PA, Rosner B, Willet WC, Stampfer MJ, et al. A population-based case-control study of carotenoid and vitamin A intake and ovarian cancer (United States). *Cancer Causes Control* 2001;**12**:83-90.
14. Bao P, Chen Z, Tai R-Z, Shen H-M, Martin FL, Zhu Y-G. Selenite-induced toxicity in cancer cells is mediated by metabolic generation of endogenous selenium nanoparticles. *J Proteome Res* 2015;**14**:1127-36.
15. Pattabiraman DR, Weinberg RA. Tackling the cancer stem cells – what challenges do they pose? *Nat Rev Drug Discov* 2014;**13**:497-512.
16. Xu W, Mezencev R, Kim B, Wang L, McDonald J, Sulchek T. Cell stiffness is a biomarker of the metastatic potential of ovarian cancer cells. *PLoS One* 2012;**7**, https://doi.org/10.1371/journal.pone.0046609.
17. Quintela M, Sieglaff DH, Gazze AS, Zhang A, Gonzalez D, Francis L, et al. HBO1 directs histone H4 specific acetylation, potentiating mechano-transduction pathways and membrane elasticity in ovarian cancer cells. *Nanomedicine* 2019;**17**:254-65.
18. Fife CM, McCarroll JA, Kavallaris M. Movers and shakers: cell cytoskeleton in cancer metastasis. *Br J Pharmacol* 2014;**171**:5507-23.
19. Suresh S. Biomechanics and biophysics of cancer cells. *Acta Materialia* 2007;**55**:3989-4014.
20. Kabla Alexandre J. Collective cell migration: leadership, invasion and segregation. *Journal of The Royal Society Interface* 2012;**9**:3268-78.
21. Bidkar AP, Sanpui P, Ghosh SS. Efficient induction of apoptosis in cancer cells by paclitaxel-loaded selenium nanoparticles. *Nanomedicine (Lond)* 2017;**12**:2641-51.
22. Liang C-C, Park AY, Guan J-L. In vitro scratch assay: a convenient and inexpensive method for analysis of cell migration in vitro. *Nature Protocols* 2007;**2**:329-33.
23. Pan-Castillo B, Gazze SA, Thomas S, Lucas C, Margarit L, Gonzalez D, et al. Morphophysical dynamics of human endometrial cells during decidualization. *Nanomedicine: Nanotechnology, Biology and Medicine* 2018;**14**:2235-45.
24. Francis LW, Gonzalez D, Ryder T, Baer K, Rees M, White JO, et al. Optimized sample preparation for high-resolution AFM characterization of fixed human cells. *Journal of Microscopy* 2010;**240**:111-21.
25. Brozmanová J, Mániková D, Vlčková V, Chovanec M. Selenium: a double-edged sword for defense and offence in cancer. *Arch Toxicol* 2010;**84**:919-38.
26. Zhao G, Wu X, Chen P, Zhang L, Yang CS, Zhang J. Selenium nanoparticles are more efficient than sodium selenite in producing reactive oxygen species and hyper-accumulation of selenium nanoparticles in cancer cells generates potent therapeutic effects. *Free Radic Biol Med* 2018;**126**:55-66.

27. Bai K, Hong B, Hong Z, Sun J, Wang C. Selenium nanoparticles-loaded chitosan/citrate complex and its protection against oxidative stress in d-galactose-induced aging mice. *Journal of Nanobiotechnology* 2017;**15**:92.
28. Zhang J, Wang H, Yan X, Zhang L. Comparison of short-term toxicity between Nano-Se and selenite in mice. *Life Sci* 2005;**76**:1099-109.
29. Clayton KN, Salameh JW, Wereley ST, Kinzer-Ursem TL. Physical characterization of nanoparticle size and surface modification using particle scattering diffusometry. *Biomicrofluidics* 2016;**10**, https://doi.org/10.1063/1.4962992.
30. Zhang JS, Gao XY, Zhang LD, Bao YP. Biological effects of a nano red elemental selenium. *Biofactors* 2001;**15**:27-38.
31 Tang HM, Kuay KT, Koh PF, Asad M, Tan TZ, Chung VY, et al. An epithelial marker promoter induction screen identifies histone deacetylase inhibitors to restore epithelial differentiation and abolishes anchorage independence growth in cancers. *Cell Death Discov* 2016;**2**:16041.
32. Wheelock MJ, Shintani Y, Maeda M, Fukumoto Y, Johnson KR. Cadherin switching. *J Cell Sci* 2008;**121**:727-35.
33. Lesniak A, Salvati A, Santos-Martinez MJ, Radomski MW, Dawson KA, Åberg C. Nanoparticle adhesion to the cell membrane and its effect on nanoparticle uptake efficiency. *J Am Chem Soc* 2013;**135**:1438-44.
34. Mierke CT. Physical break-down of the classical view on cancer cell invasion and metastasis. *Eur J Cell Biol* 2013;**92**:89-104.
35. Tadeo I, Berbegall AP, Escudero LM, Alvaro T, Noguera R. Biotensegrity of the extracellular matrix: physiology, dynamic mechanical balance, and implications in oncology and mechanotherapy. *Front Oncol* 2014;**4**:39.
36. Cross SE, Kreth J, Zhu L, Sullivan R, Shi W, Qi F, et al. Nanomechanical properties of glucans and associated cell-surface adhesion of Streptococcus mutans probed by atomic force microscopy under in situ conditions. *Microbiology (Reading, Engl)* 2007;**153**:3124-32.
37. Zhai Q, Xiao Y, Li P, Tian F, Zhao J, Zhang H, et al. Varied doses and chemical forms of selenium supplementation differentially affect mouse intestinal physiology. *Food Funct* 2019;**10**:5398-412.
38. Xia Y, Chen Y, Hua L, Zhao M, Xu T, Wang C, et al. Functionalized selenium nanoparticles for targeted delivery of doxorubicin to improve non-small-cell lung cancer therapy. *Int J Nanomedicine* 2018;**13**:6929-39.
39. Lara-Cruz C, Jiménez-Salazar J, Ramón-Gallegos E, Damian-Matsumura P, Batina N. Increasing roughness of the human breast cancer cell membrane through incorporation of gold nanoparticles. *Int J Nanomedicine* 2016;**11**:5149-61.
40. Oh N, Park J-H. Endocytosis and exocytosis of nanoparticles in mammalian cells. *Int J Nanomedicine* 2014;**9**:51-63.
41 Ganyc D, Self WT. High affinity selenium uptake in a keratinocyte model. *FEBS Lett* 2008;**582**:299-304.
42. Janel S, Popoff M, Barois N, Werkmeister E, Divoux S, Perez F, et al. Stiffness tomography of eukaryotic intracellular compartments by atomic force microscopy. *Nanoscale* 2019;**11**:10320-8.
43. Wang Y, Xu C, Jiang N, Zheng L, Zeng J, Qiu C, et al. Quantitative analysis of the cell-surface roughness and viscoelasticity for breast cancer cells discrimination using atomic force microscopy. *Scanning* 2016;**38**:558-63.